Research Article

Effect of Inhomogeneous Mechanical Properties on the Stress-Strain Field at the Crack Tip and Crack Growth Direction in Dissimilar Metal Welded Joints

Shuang Wang [ID],[1,2] **Hongkui Zhang** [ID],[1,2,3] **Zhe Ju** [ID],[1] **Bing Li** [ID],[1] **Fandong Chen** [ID],[1] **and Fei Han** [ID][1,2]

[1]*Fushun CCTEG Testing Center Co., Ltd, Fushun, Liaoning 113122, China*
[2]*CCTEG Shenyang Research Institute, Fushun, Liaoning 113122, China*
[3]*State Key Laboratory of Coal Mine Safety Technology, Fushun, Liaoning 113122, China*

Correspondence should be addressed to Shuang Wang; wangshuang@syccri.com

In the failure analysis and safety assessment of dissimilar metal welded joints, the mechanical heterogeneity of local regions is usually ignored and limited sampling locations are selected. The mechanical behavior of the crack tip region is the main variables affecting the environmentally assisted cracking behavior, and it is crucial for understanding the impact of mechanical heterogeneity on the local stress-strain state at the crack tip in welded joints. In this study, the effect of mechanical heterogeneity on the local mechanical behavior at the crack tip and on the stress-strain condition at the crack tip front for different crack sizes was investigated through finite-element simulations based on user-defined material subroutines. The local mechanical behavior of an interface region and crack propagation direction with mechanical heterogeneity and a series of initial crack locations were analyzed. The results show that mechanical heterogeneity has a significant effect on the mechanical condition and growth path of cracks at different sampling locations. The interaction between the mechanical heterogeneity around the crack and the crack depth determines the stress and plastic strain in front of the crack tip, which causes a substantial change in the crack growth path. The interface cracks have high stress and plastic strain; thus, the interface is often the weak position where damage occurs. To guarantee a reliable integrity assessment of cracks in mechanically heterogeneous interface regions, local mechanical properties related to crack locations should be determined and utilized.

1. Introduction

Dissimilar metal welded joints (DMWJs) are used to connect pressure-bearing equipment to the main pipeline in the primary water systems of pressurized water reactors. The mechanical properties of the local regions in welded joints are heterogeneous because of the inherent properties of joints [1]. Studies have shown that DMWJs are often the weak components wherein damage occurs and are the most susceptible to stress corrosion cracking (SCC) [2–4]. The mechanical condition at the local crack tip region is a significant factor affecting the environmentally assisted cracking (EAC) behavior, which compromises the safety performance of metal structures and may lead to catastrophic accidents [1, 4, 5].

Therefore, it is crucial to analyze the local stress-strain behavior of crack tips in mechanically heterogeneous DMWJs when performing an accurate structural integrity assessment.

The inherent properties of welded joints entail inhomogeneities in the mechanical and material properties of the local regions, which have a significant impact on the integrity assessment of welded structures [1]. Furthermore, fracture resistance, mechanical properties, and microstructure, which are highly heterogeneous along DMWJs, have restricted a more detailed evaluation of the DMWJs [6, 7]. When a single material mechanical property or a simple partitioned sandwich model is used to analyze for nonhomogeneous welded joints, the results are often inaccurately predicted, resulting in a less detailed estimate of the loading

capacity of welded structures [8]. When conducting a DMWJ integrity analysis, it is important to consider the impact of local strength inhomogeneities on fracture behavior. Specifically, it is essential to focus on any differences in material properties between the joint materials and any sudden changes in mechanical properties across narrow areas of the weld. Existing methods for integrity assessment of DMWJs often overlook the impact of the heat-affected zone (HAZ) and fusion zone (FZ) [9]. The commonly used simplistic multimaterial models do not directly assess the mechanical characteristics of strength-mismatched welded joints, which may influence the reliability of calculations based on such models. Sandwich composite structures are often used in engineering applications in which the mechanical heterogeneity of DMWJs is considered [10–12]. Despite their exceptional structural characteristics, such structures exhibit mismatched interregional material and geometric features [13, 14]. The variation in interfacial stresses due to mechanical loading is significant at each regional interface [15, 16]. Consequently, in the case of simplified sandwich structures, it becomes difficult to characterize the HAZ and FZ, the two weakest zones in a DMWJ, in detail [17]. To conduct a detailed failure analysis of DMWJs, it is therefore necessary to elucidate the mechanical behavior of all regions in welded joints, especially the interface regions with mechanical heterogeneities [18]. Guo et al. [19] provided a suitable expression of mechanical inhomogeneity by using a temperature field approach in the analysis of the mechanical state of the interface crack tip. That is, different temperatures were set in different regions throughout the model, and each temperature then corresponded to one material mechanical property. The mechanical heterogeneity of the welded joint is expressed by means of the temperature field, and the results show that this is only an approximate expression and is not well suited to meet more detailed characterization. Wang et al. [3, 20, 21] conducted a numerical simulation of the local fracture resistance of DMWJs by simplifying the interface areas, i.e., by ignoring the mechanical heterogeneity of the local regions. The crack locations selected in these studies were limited. However, cracks may arise at random positions in welded joints during service [22]. When initial cracks appear at different positions in the interface region, the resulting heterogeneity will inevitably affect the local stress-strain condition at the crack tip and the crack growth path. Zhao et al. [23] discussed the effect of mechanical heterogeneities on the stress-strain field and stress triaxiality at the crack fronts of semielliptic surfaces. They reported that the interaction between the strength heterogeneity and crack depth directly affects the direction of crack propagation. Meanwhile, this inhomogeneous state, in turn, affects the crack tip's mechanical properties and drives crack growth. Therefore, selecting suitable crack tip mechanical field parameters to assess the fracture behavior is worthy of an in-depth study. However, the mechanical behavior of the crack tip in a mechanically heterogeneous DMWJ, considering a series of different initial crack locations, has not been systematically studied or understood.

In this study, the finite-element method (FEM) based on user-defined material (UMAT) subroutines was used to study the effect of mechanical heterogeneity on the mechanical behavior at the crack tip. The variation in mechanical properties in the interface regions of SA508/52 Mb, 52 Mb/52 Mw, and 52 Mw/316 L was investigated through experiments and numerical simulations. The effect of mechanical heterogeneity on the stress and plastic strain at the crack tip in the interface regions and the stress-strain condition at the crack tip front was analyzed considering different crack lengths. Finally, the mechanical behavior of the crack tip at different positions in the welded structure was assessed.

2. Materials and Methods

2.1. Material Constitute Model and Computer Code Implementation. The "linear isotropic hardening" material constitutive model for plastic behavior is implemented into the ABAQUS code through the UMAT subroutine. This subroutine can be utilized to describe the mechanical behavior of materials and conduct computations at various integration points [24]. The mechanical properties of these integration points are reflected point-by-point to the various locations to more accurately identify the mechanical characteristics at various places. This subroutine is composed of two major components: the elastic trial and the return mapping. The UMAT calculates the elastic trial stress ($\sigma_{n+1}^{\text{trial}}$) at time ($t_{n+1}$) and compares it with the difference in the yield function (f_{n+1}^{trial}); the result determines whether the stress reaches the plastic stage. When $f_{n+1}^{\text{trial}} \leq 0$ is reached, the integration process is in the elastic stage. Furthermore, since the plastic strain increment ($\Delta\varepsilon_p$) is equal to zero, the total strain increment ($\Delta\varepsilon$) reflects the elastic strain increment ($\Delta\varepsilon_e$), and the elastic stiffness matrix (D_e) is used to obtain the stress at t_n to t_{n+1}. When $f_{n+1}^{\text{trial}} > 0$, on the other hand, the integration process reaches the plastic stage. Thus, $\Delta\varepsilon_p$ is greater than zero, and $\Delta\varepsilon$ is divided into $\Delta\varepsilon_e$ and $\Delta\varepsilon_p$. Furthermore, for a stress reaching the plastic state, the elastic-plastic stiffness matrix (D_{ep}) is used to obtain the stress at t_n to t_{n+1}. This subroutine includes the calculation of trial stress and equivalent stress, calculation of plastic strain, and update of the state variables.

When there is an applied load, the total strain increment is divided into the following components:

$$\Delta\varepsilon = \Delta\varepsilon_e + \Delta\varepsilon_p. \tag{1}$$

Assuming a purely elastic initial condition, the trial stress may be defined as follows:

$$\sigma_{n+1}^{\text{trial}} = \sigma_n + D_e : \Delta\varepsilon_e, \tag{2}$$

where trial represents the trial state and D_e is the Jacobi matrix in the elastic state, i.e.,

$$D_e = \frac{E}{2(1+\nu)}\left(\delta_{ik}\delta_{jl} + \delta_{il}\delta_{jk}\right) + \frac{\nu E}{(1+\nu)(1-2\nu)}\left(\delta_{ij}\delta_{kl}\right), \tag{3}$$

where E represents Young's modulus and v represents Poisson's ratio. δ_{ij} denotes the abbreviation for the unit matrix, when $i = j$, $\delta_{ij} = 1$; when $i \neq j$, $\delta_{ij} = 0$.

The yield function can be represented as

$$f(\sigma_{ij}, k) = 0, \tag{4}$$

where f is referred to as the yield function and k is a constant associated with the material. The surface where $f = 0$ is termed the yield surface.

Following that, the equivalent stress $\overline{\sigma}$ can be described as follows [24]:

$$\overline{\sigma} = \sqrt{\frac{3}{2}} \|S\|, \tag{5}$$

where S denotes the deviatoric stress.

Using the J_2 rule as a guide [25],

$$\Delta\varepsilon_p = \Delta\lambda \frac{3S}{2\overline{\sigma}}, \tag{6}$$

where $d\lambda$ is the classical plastic multiplier.

Then, ε_{n+1}^p at t_{n+1} is

$$\varepsilon_{n+1}^p = \varepsilon_n^p + 1.5\Delta\lambda \frac{s_{n+1}^{\text{trial}}}{\overline{\sigma}_{n+1}^{\text{trial}}}. \tag{7}$$

The plastic multiplier being equal to the equivalent plastic strain increment is due to the choice of a Mises material. Hence, the equivalent plastic strain increment is

$$\Delta\varepsilon_n^p = \Delta\lambda = \frac{\sigma_{n+1}^{\text{trial}} - \sigma_y}{H + 3G}, \tag{8}$$

where H is the tangential modulus, G is the shear modulus and $G = E/2(1 + v)$, and σ_y is the yield strength.

In the UMAT subroutine, updating the stress requires using separate methods for the elastic and plastic phases. When the stress is in the elastic state, the stress increment can be described as follows:

$$d\sigma = D_e(d\varepsilon - d\varepsilon_p). \tag{9}$$

Note that $d\varepsilon_p$ is an equivalent plastic strain increment $\Delta\varepsilon_n^p$.

However, when the stress exceeds the elastic state,

$$d\sigma = D_{ep}d\varepsilon, \tag{10}$$

where $D_{ep} = D_e - D_p$, in which $D_p = 9G^2 * S * S^T / \overline{\sigma}^2 (H + 3G)$ [26, 27].

2.2. Determination of Mechanical Parameters.

It is difficult to achieve equal strength in the base metal (BM) and weld metal (WM) zones of DMWJs, and strength heterogeneity generally exists [28]. The results obtained using standard material structural safety assessment methods are either not sufficiently conservative or are excessively conservative for predicting the fracture behavior of welded structures, to the extent that it becomes difficult to satisfy the requirements of practical engineering applications [21]. Therefore, to determine the local mechanical parameters of DMWJs, the

welded joint at the safety end of a nuclear power circuit was taken as an example in this study. To properly simulate the DMWJs, the filler metal was modeled using Alloy52 M, and low-alloy steel SA508 and austenitic stainless steel 316L were used to form BM. Buttering Alloy52 Mb (52 Mb) and weld Alloy52 Mw (52 Mw) formed the weld metal. The inner wall had a 304 L stainless steel (SS) overlay. The structure is shown in Figure 1(a), and the geometry is shown in Figure 1(b) in mm. The inner pipe diameter is 834.6 mm, the outer pipe diameter is 1001.6 mm, the pipe wall thickness is 83.5 mm, and the wall thickness of the fusion cladding layer is 8.5 mm.

The specimens were polished to 2.5 μm, and the variation in the hardness at different locations of the DMWJs was measured using an HVS-1000Z digital display microhardness tester. The measurement was performed along the straight line L1 shown in Figure 2. The load was 200 g, and the holding time was 15 s.

The mechanical property distribution in the middle part of the model as shown in Figure 3 was selected as the material parameter for this FEM numerical simulation experiment modeling. A continuous indentation test was performed across the specimen. Starting from the SA508 area, moving perpendicularly to the weld direction through the 52 M area, and ending at the 316L area, this process aimed to obtain local Vickers hardness. Figure 2 illustrates the locations of the indentation test. In addition, Figure 3 presents a scatter plot showcasing the distribution of the Vickers hardness in the horizontal direction.

Based on the approach described in [29], the relationship between yield strengths and the hardness in BM, HAZ, and WM can be expressed using equation (9). The hardness values obtained experimentally for each region were converted to yield strength, and the mechanical heterogeneous field distribution curves are shown in Figure 4.

$$\sigma_y = \begin{cases} 3.28\text{HV} - 221 & (\text{BM, HAZ}) \\ 3.15\text{HV} - 168 & (\text{WM}) \end{cases}. \tag{11}$$

2.3. Material Model

2.3.1. Material Model of Sandwich Composite Structure.

In the traditional study of the mechanical properties of the welded joint local area, the welded joint is usually simplified to a multimaterial model, often without considering the mechanical heterogeneous HAZ and FZ, each region is (such as different colors in Figure 5) assigned to the respective mechanical properties of the material, ignoring the phenomenon of abrupt changes in mechanical properties of the interface region of dissimilar materials. Although this analysis method is simple, it can lead to inaccurate results and make it difficult to accurately analyze the structural integrity of welded joints. The "sandwich" material model is shown in Figure 5.

The DMWJ in this study consists of a base material (low-alloy steel SA508 and austenitic stainless steel 316L) and a weld material (Alloy52 M). According to [20, 21] and the results of the tests on yield strength in this work, the mechanical properties of the four materials at room temperature were analyzed and obtained as shown in Table 1. This

(a)   (b)
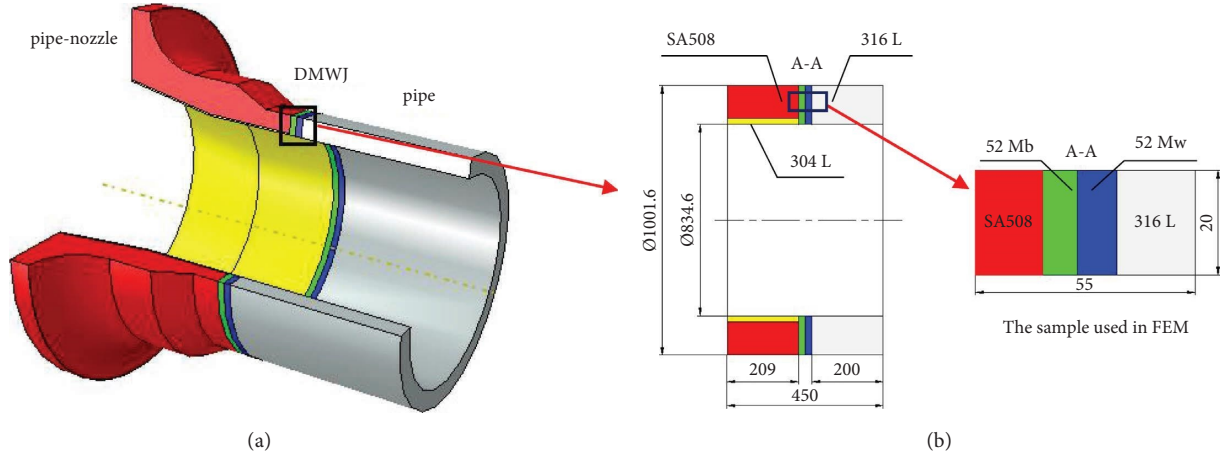
Figure 1: Dissimilar metal welded joint (DMWJ). (a) Typical dissimilar welded joint. (b) Four materials constituting the DMWJ and sample used in FEM.
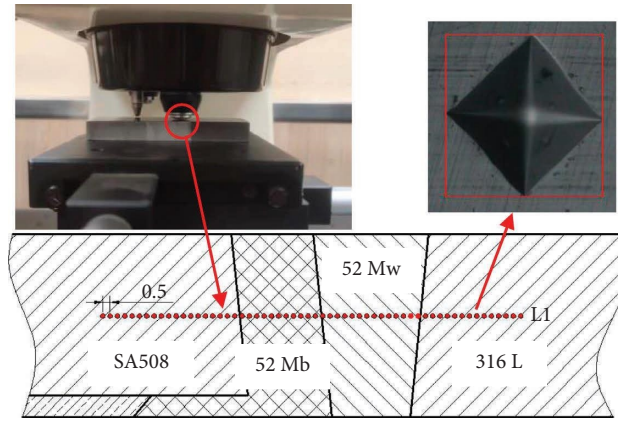

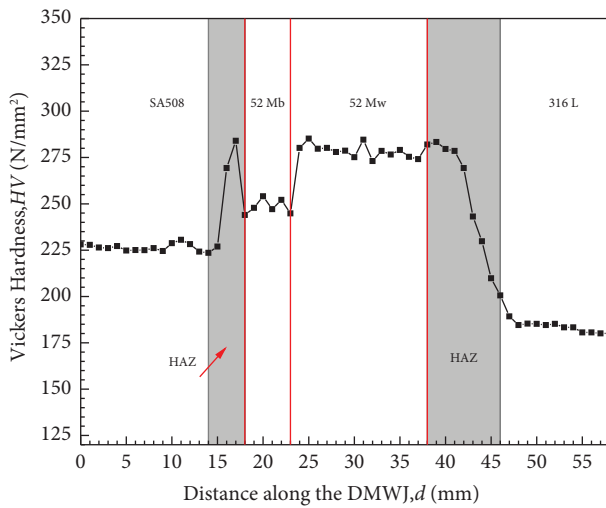Figure 2: HVS-1000Z type digital display microhardness tester measuring hardness.

Figure 3: Vickers hardness distribution along DMWJ.

material's mechanical property is assigned to the sandwich model.

2.3.2. Continuous Transition Material Model. To avoid abrupt changes in mechanical properties in the interface region of dissimilar materials caused by the sandwich model, this study assigns the continuously transitioned material mechanical properties to the numerical model through the subroutine UMAT, as shown in Figure 4(b), so that the mechanical properties distributed along the welded joint correspond to the spatial location one by one, thus achieving a continuous distribution of mechanical properties.

When $\sigma \leq \sigma_y$, elastic deformation occurs; when $\sigma > \sigma_y$, plastic deformation occurs, and the expression is

$$\sigma = \begin{cases} E\varepsilon_e, & \sigma \leq \sigma_y, \\ \sigma_y + H\varepsilon_P, & \sigma > \sigma_y, \end{cases} \tag{12}$$
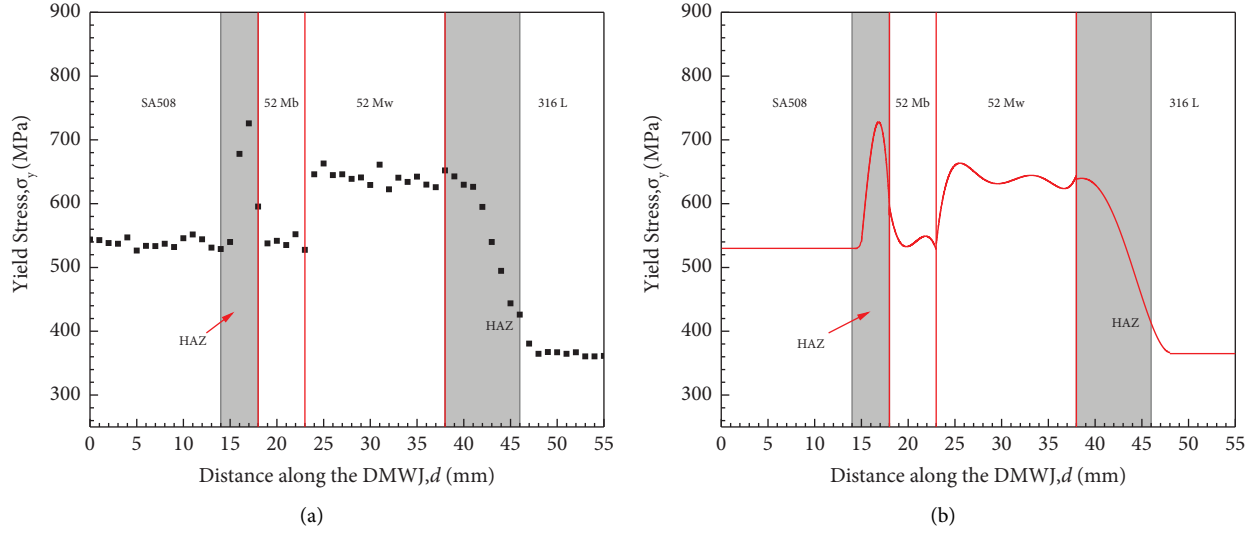
FIGURE 4: Mechanical heterogeneous field distribution of the DMWJ. (a) Yield strength distribution. (b) Yield strength fitting curve.
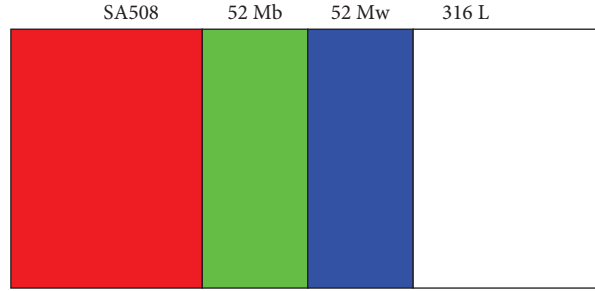

FIGURE 5: Sandwich composite structure model.

TABLE 1: Mechanical properties of materials for the sandwich model.

Materials	Young's modulus E (MPa)	Poisson's ratio v	Yield strength σ_y (MPa)	Hardening coefficient H (MPa)
SA508	202410	0.3	540	1200
52Mb	178130	0.3	527	415
52Mw	178130	0.3	635	481
316L	202000	0.3	365	435

where σ is the stress, ε_e is the elastic strain, and σ_y is the yield strength; furthermore, H' denotes the hardening coefficient during the plastic deformation state.

The axial direction is used as the y-direction. The yield function $\sigma_y(y)$ and the hardening function $H(y)$ vary with position.

$$\sigma_y = \begin{cases} E\varepsilon_e, & \sigma \leq \sigma_y, \\ \sigma_y(y) + H(y)\varepsilon_P, & \sigma > \sigma_y. \end{cases} \tag{13}$$

y in the parentheses represents different positions. When using the UMAT subroutine to express the mechanical heterogeneity of the DMWJ, it is necessary to define E, v, $\sigma_y(y)$, and $H(y)$ at various locations across the DMWJ.

Based on hardness test results, the yield strength of the continuous transition was fitted, and the fitted curve is shown in Figure 4(b). Dissimilar metal welded joint local area yield strength fitting function $\sigma_y(y)$ is shown in equation (12), and the correlation coefficient $R = 0.99$.

$$\sigma_y(y) = \begin{cases} 540, & (0, 15) \\ 47493.6996 - 9715.126y + 659.0416y^2 - 14.67y^3, & (15, 18) \\ 34974.10086 - 4981.27488y + 239.6228y^2 - 3.83309y^3, & (18, 23) \\ 635, & (23, 38) \\ 128248.41352 - 13048.87804y + 495.93277y^2 - 8.29737y^3 + 0.05151y^4, & (38, 48) \\ 365, & (48, 55), \end{cases}$$
$$(14)$$

$$H(y) = \frac{\sigma_u - \sigma_y(y)}{\Delta\varepsilon_p},$$

where the study focuses on the analysis of the crack tip mechanical field distribution under the inhomogeneous distribution of yield strength. Therefore, σ_u of the four materials is constant at 650 MPa, 500 MPa, 530 MPa, and 550 MPa, respectively [20].

2.4. Specimen Geometry and Crack Locations.

A simplified schematic of the DMWJ used in the FEA is shown in Figure 6. Mechanical characteristics substantially vary nearer to the interface; moreover, the properties of HAZ are uneven owing to the effects of welding [30]. A straight interface was utilized in the simulation for purposes of understanding.

To demonstrate that the "continuous transition" model can accurately characterize the continuous change in material mechanical properties along the welded joint, the model without prefabricated cracks was simulated in tension and compared with the "sandwich" model. Subsequently, the crack tip mechanical fields of the SA508/52 Mb interface crack, 52 Mb/52 Mw interface crack, and 52 Mw/316L interface crack were analyzed in detail, respectively. Finally, the cracks were placed at different positions in the interface regions to accurately analyze the stress-strain condition at the crack tips at different positions of the DMWJ and to determine the local mechanical behavior of the two interface regions. In Figure 7, y represents the distance between the crack and the interfaces (which include the SA508/52 Mb interface and the 52 Mw/316 L interface), with $y = 0$ at the interface.

2.5. Mesh Model and Boundary Condition.

Axisymmetric models are generally recognized as being suitable for modeling the welding of cylindrical structures to evaluate the local mechanical properties of DMWJs, despite the fact that welding is a three-dimensional operation [31]. Therefore, in this study, finite-element simulations, a relatively fast and convenient method widely used with finite-element models, were performed to evaluate the local stress-strain behavior of DMWJ crack tips with mechanical heterogeneity. Specifically, two finite-element models were used in ABAQUS software: (a) a model without prefabricated initial cracks and (b) a model with prefabricated initial cracks.

(1) The left end of the model (a) was fixed, and a displacement load of 0.5 mm was applied to the right end. The reasonability of the method in terms of characterizing the mechanical heterogeneity was demonstrated by comparing the aforementioned model with a simplified sandwich structure, as shown in Figure 8(a).

(2) Based on the demonstration that the continuous transition model can characterize the non-homogeneous material mechanical properties distributed along the welded joint. A model with prefabricated cracks was reestablished (b). There was a seam crack, with crack tip singularity described by a 0.25 midside node parameter and collapsed element side. The load K_I (30 MPa·m$^{1/2}$) was applied to the model (b) using a laboratory simulation of a light water reactor environment to study the effect of mechanical heterogeneity on the local mechanical behavior at the crack tip, as shown in Figure 8(b) [1]. Within the local area of the crack tip ($r = 0.1$ mm), the crack tip mesh was refined with an approximate element size of 0.005, and a structured partition was used. Four-node bilinear axisymmetric elements (CAX4) were used in the mesh elements. The K_I application was achieved by applying a load σ.

$$K_I = \sigma\sqrt{\pi a}f\left(\frac{a}{h}\right),$$

$$f\left(\frac{a}{h}\right) = 1.12 - 0.23\left(\frac{a}{h}\right) + 10.6\left(\frac{a}{h}\right)^2 - 21.71\left(\frac{a}{h}\right)^3 + 30.38\left(\frac{a}{h}\right)^4,$$
$$(15)$$

where a is the initial crack length and h is the model width.

The inclusion crack model (ii) in Figure 8(b) always keeps the crack position unchanged, avoiding the introduction of the geometric constraint, and realizes the change of the crack position relatively by moving the mechanical properties of the material, as shown in Figure 9. Instead of partitioning, the mechanical properties of the material corresponding to the different positions can be realized by simply using the UMAT subroutine, thus
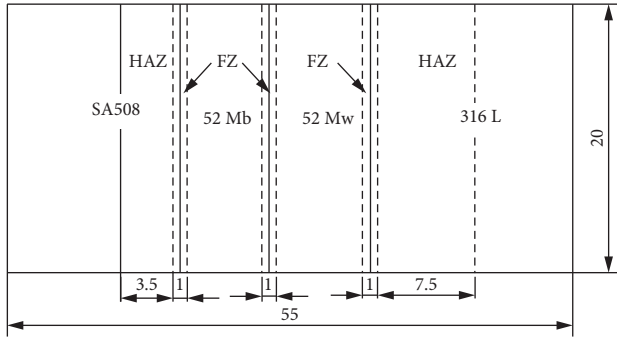
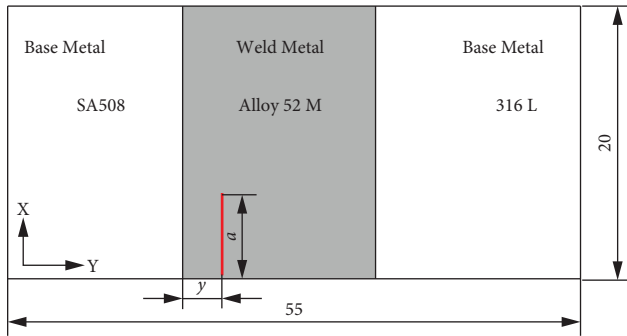Figure 6: Simplified schematic of the welded structure.

Figure 7: Specimen geometry and crack locations.

achieving the effect of analyzing only mechanical heterogeneity on the mechanical behavior of the crack tip.

3. Results and Discussion

3.1. Analysis of Results of the Continuous Transition Model and Sandwich Composite Structure. For actual welded joints, the strength, hardening properties, and inherent toughness of each material (BM and WM) constituting the interface zone are different. Mismatches in strength, hardening, and inherent material toughness exist simultaneously, and they mutually determine the level of the material constraint in the interface region. Previous studies on the mechanical properties of welded joints have generally used a sandwich structure, ignoring the effects of HAZ and FZ. The result is a sandwich structure with significant and abrupt changes in mechanical properties at the interface, which cannot satisfy practical engineering requirements. Meanwhile, the method used in this study considers the existence of HAZ and FZ and can thus accurately reflect the mechanical properties of a DMWJ at different positions. The results of the observations along L2 in the model (i) are shown in Figure 10. Stress increases at the interface region as a result of the hardening of HAZ and FZ, while the equivalent plastic strain (PEEQ) decreases. In traditional methods of analyzing welded joints, multimaterial welded joints are usually simplified to a single material straight pipe for analysis. If the material strength value used is too low, the resulting safety value is smaller than the actual safety value, which tends to produce an overconservative (oversafe) assessment, resulting in a waste of available resources; if the material strength value used is

too high, the resulting safety value is larger than the actual safety value, which tends to produce an unconservative (unsafe) assessment and cause safety accidents. The continuous transition model proposed in this study describes more accurately the mechanical properties at different positions and avoids nonconservative or overconservative results, as shown in Figure 10. Therefore, it is more appropriate for evaluating the integrity of DMWJ as compared to the simpler composite structure [32].

3.2. Stress-Strain Condition of the Crack Tip at the Interface. Mechanical variables such as stress and plastic strain at the crack tip are generally used for assessing EAC behavior. Therefore, we analyzed the impact of mechanical heterogeneity on the local mechanical parameters at the crack tip and discussed the stress and plastic strain under a constant K_I (30 MPa m$^{1/2}$), as determined via a laboratory simulation of a light water reactor environment [1].

In this section, the stresses and plastic strains at the crack tip ($a = 10$ mm) for the three interfaces, SA508/52 Mb, 52 Mb/52 Mw, and 52 Mw/316L, will be discussed separately. In Figure 7, the stresses and plastic strains at the crack tips on both sides of the weld are shown. The maps are divided into 7 areas by 6 contours. The stresses at the crack tip are shown in Figure 11(a), with the 6 contours corresponding to stresses of 300, 400, 500, 600, 700, and 800 MPa. The PEEQ of the crack tip is shown in Figure 11(b), with the 6 contours representing strains of 0.1%, 0.25%, 0.5%, 1.0%, 1.5%, and 2.0%. In addition, it has been utilized to clarify the impact of mechanical heterogeneity on the stress and plastic strain near the crack tip.

Figure 11 shows the distributions of the von Mises stress and PEEQ of the crack tip at the SA508/52 Mb interface in mechanically heterogeneous welded joints. The strength distribution of the SA508/52 Mb interface region is shown in Figure 4. The yield strength in the HAZ of SA508 is significantly higher than that of 52 Mb; therefore, the stress in SA508 is greater than that in 52 Mb. By contrast, the strain in 52 Mb is significantly higher than that in SA508. These results suggest that there may be a larger change in stress at the crack tip as the strength increases. Moreover, as the yield strength decreases, a steep gradient in the PEEQ at the crack tip appears.

Figure 12 shows the von Mises stress and PEEQ of the crack tip at the 52 Mb/52 Mw interface in mechanically heterogeneous welded joints. Since the yield strength of 52 Mb is significantly less than that of 52 Mw, the stress in 52 Mb is less than that in 52 Mw. Similarly, the strain in the 52 Mb side is significantly larger than that in the 52 Mw side. These findings demonstrate that the distribution of stress and plastic strain at the crack tip in mechanically heterogeneous welded joints is extremely heterogeneous. The heterogeneous distribution of stress and strain may cause changes in the direction of crack growth.

Figure 13 shows the von Mises stress and PEEQ distributed at the crack tip in the 52 Mw/316L interface of the mechanically heterogeneous welded joint. The strength distribution of the 52 Mw/316L interface region is shown in
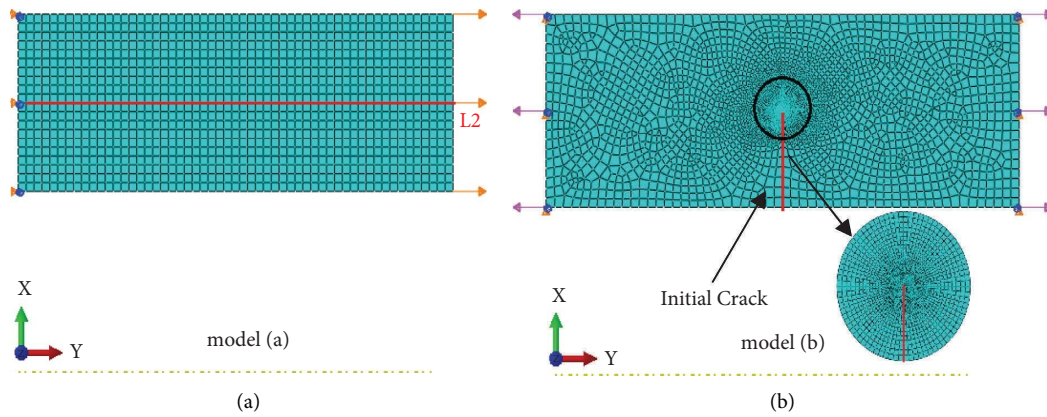
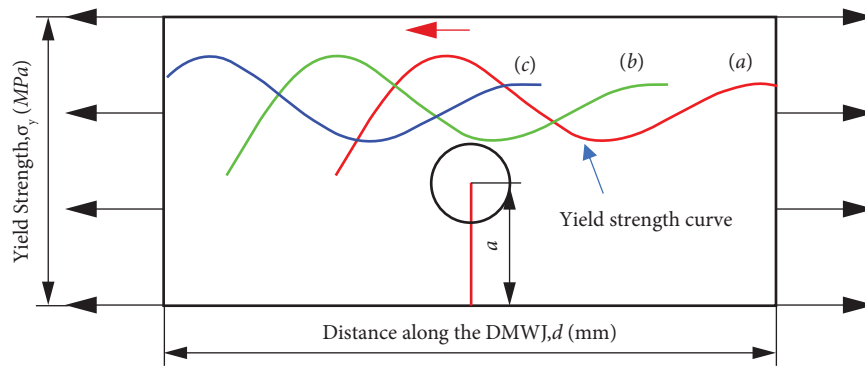FIGURE 8: Mesh models (a) without prefabricated cracks and (b) with prefabricated cracks.

FIGURE 9: The distribution of the mechanical properties of the material when analyzing 3 different interface cracks. (a) The distribution of material mechanical properties when analyzing the SA508/52Mb interface crack. (b) The distribution of material mechanical properties when analyzing the 52Mb/52Mw interface crack. (c) The distribution of material mechanical properties when analyzing the 52Mw/316L interface crack.
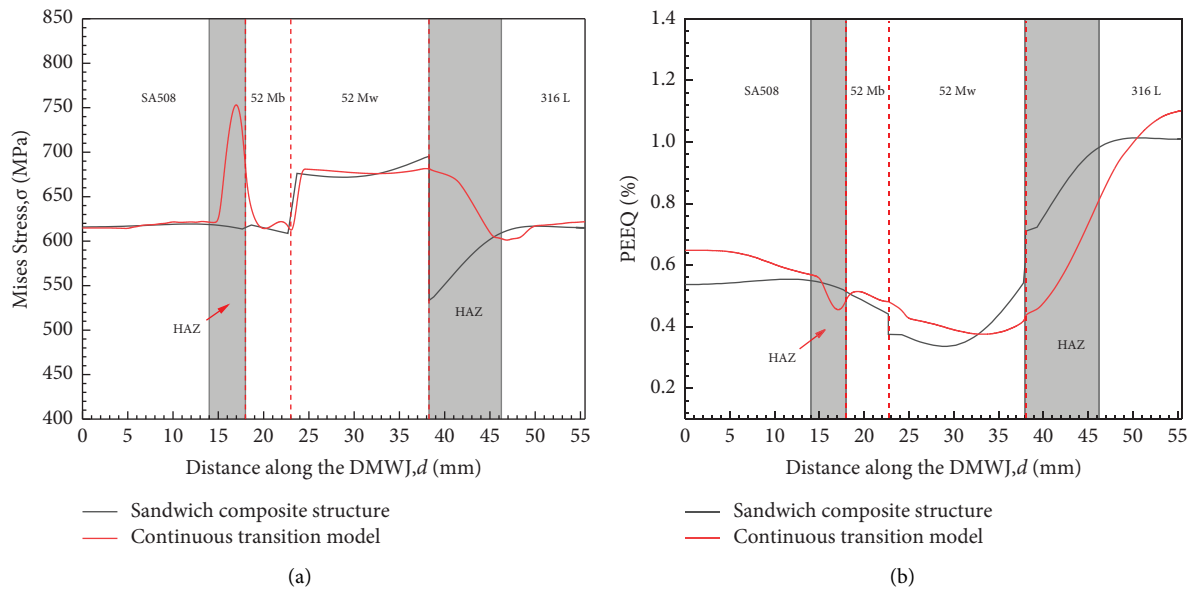

FIGURE 10: Stress-strain distribution along the DMWJ: (a) von Mises stress distribution; (b) equivalent plastic strain.
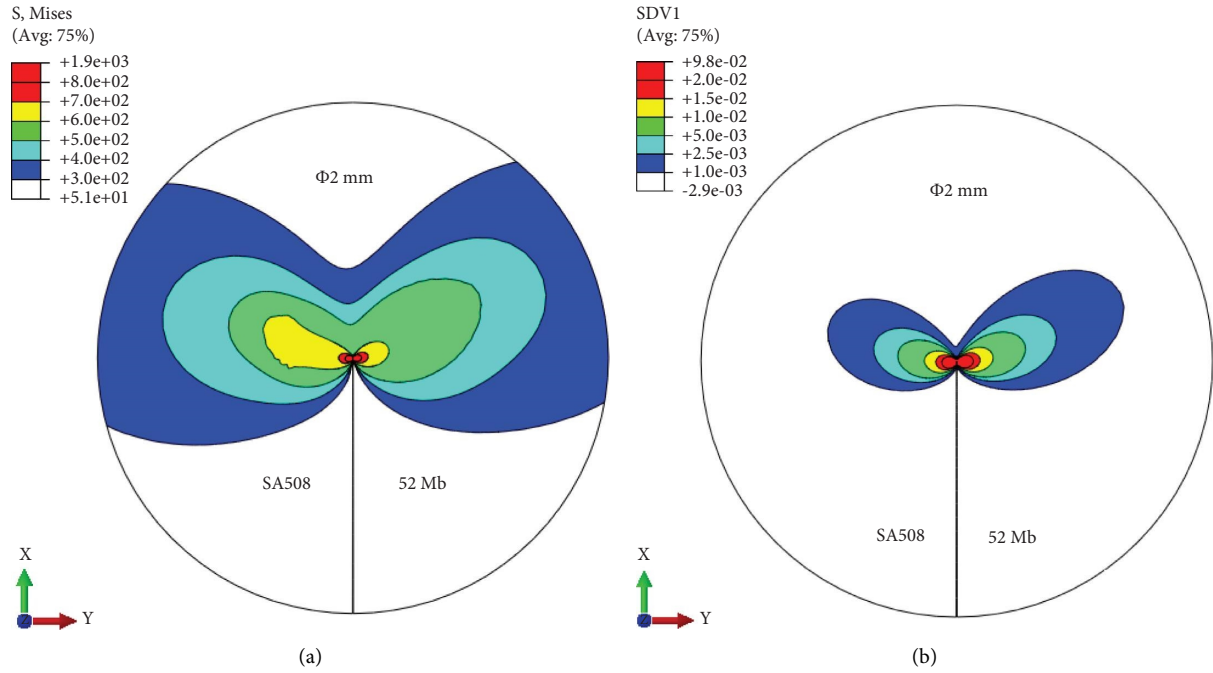
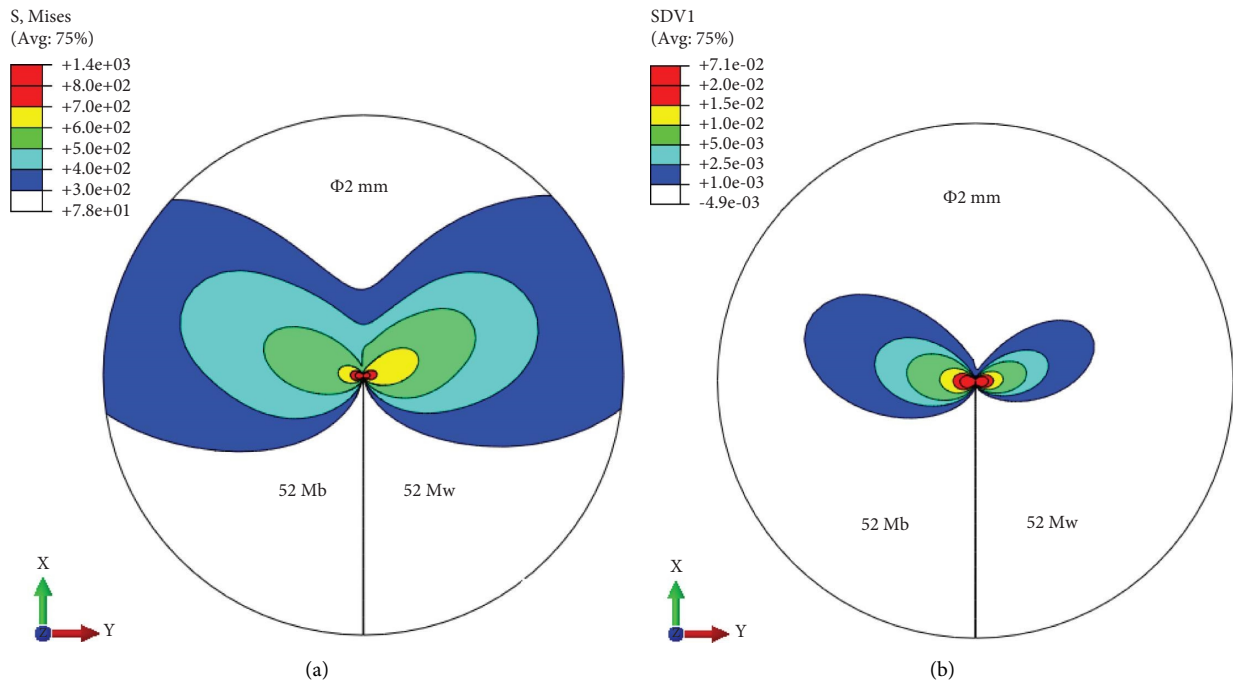FIGURE 11: SA508/52Mb interface crack tip: (a) von Mises stress; (b) PEEQ.

FIGURE 12: 52Mb/52Mw interface crack tip: (a) von Mises stress; (b) PEEQ.

Figure 2. The difference in yield strength between the local regions on the two sides of the 52 Mw/316L interface is small; hence, the stress and PEEQ distribution have no significant difference. These findings show that the stress and PEEQ on the two sides of the interface are approximately symmetrically distributed in the local region when the differences in the mechanical properties of the materials are not significant.

3.3. Stress and Strain at a Certain Distance in front of the Crack Tip.
In this section, the magnitude of stress and strain at different crack depths at a certain distance ($r = 0.5$ mm) ahead of the crack tip for the three interfaces, SA508/52 Mb, 52 Mb/52 Mw, and 52 Mw/316L, will be discussed separately. The crack tip is taken as the center of the circle, and the circle is drawn with $r = 0.5$ m; the data points are selected from the nodes on the circumference of the circle. As shown in
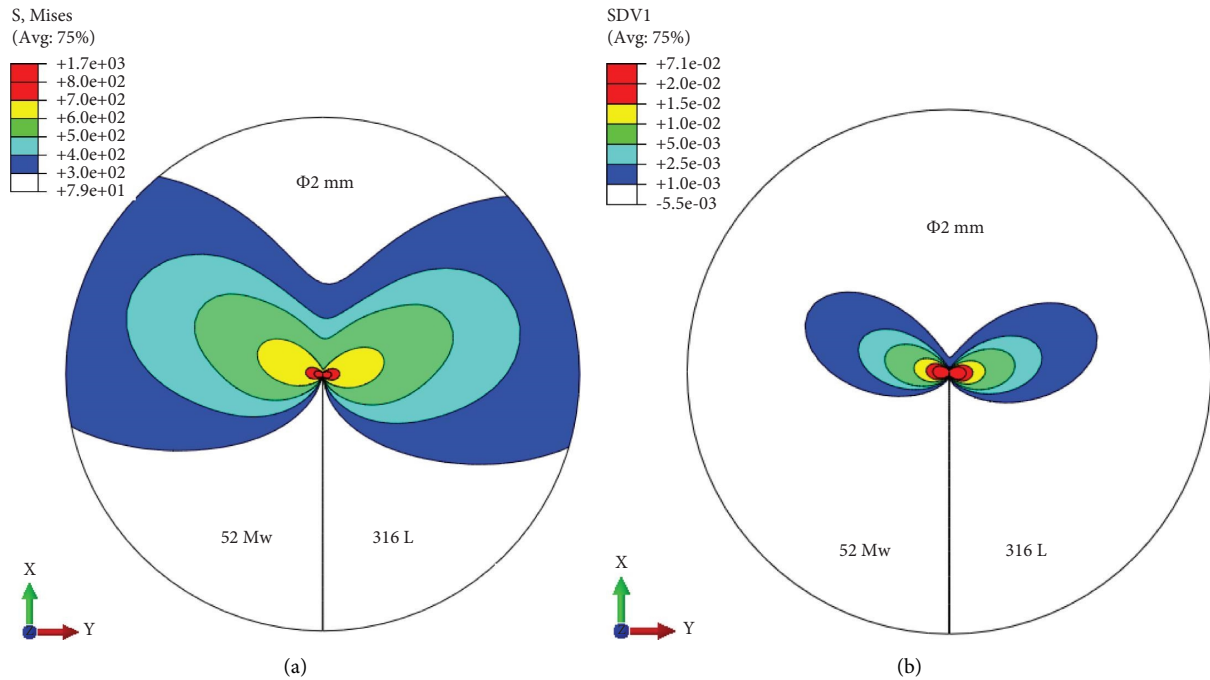
FIGURE 13: 52Mw/316L interface crack tip: (a) von Mises stress; (b) PEEQ.

Figure 14, the direction along the crack tip is taken as 0°. After obtaining the stress-strain magnitudes at a certain distance ahead of the crack, the direction of further possible deflection of the crack was decided according to the magnitudes of the stress and strain in the local area of the crack tip, as shown in Figure 15.

In this section, the stress-strain magnitudes at a certain distance ($r = 0.5$ mm) in front of the crack tip for crack depths of 5.0, 7.5, and 10.0 mm are discussed. The effect of crack depth on the mechanical field of the interfacial crack tip and the crack propagation direction was analyzed. Figure 16 shows the magnitude of the crack tip front stress and PEEQ at the SA508/52 Mb interface. As the crack depth increases, the stress and strain at the crack tip increase, and the higher stress and strain further promote the initiation and growth of ductile cracks. Because the yield strength of the SA508 side near the interface is higher than that of the 52 Mb side, the stress in SA508 is slightly higher than that in 52 Mb; this effect gradually becomes more evident as the crack size increases. The equivalent plastic strain exhibits the opposite trend. A typical example is when $a = 10$ mm, at which the crack growth is dominated by stress; moreover, the stress values are 584.829 MPa and 555.494 MPa when the angles between the taking point and the crack are −58° and 68°, respectively. If initial crack growth occurs at the SA508/52 Mb interface, the crack is likely to grow in the direction of −58° or 68° from the initial crack angle and the crack is more likely to propagate to the SA508 side, as shown in Figure 16(a). When crack growth is dominated by the equivalent plastic strain, the analysis method remains the same, and the crack is likely to grow in the direction of −58° or 68° from the initial crack angle; the crack is more likely to propagate to the 52 Mb side, as shown in Figure 16(a).

Generally, when the equipment undergoes start-stop or one overload, crack growth is dominated by strain; when the equipment operates stably, the load continues to remain constant and crack growth is often dominated by stress. In engineering applications, the corresponding stress or strain dominance can be selected based on the operating state of the equipment.

Figure 17 shows the magnitude of the crack tip stress and the PEEQ at the 52 Mb/52 Mw interface. The stress on the 52 Mw side is slightly higher than that on the 52 Mb side, and the magnitude of the stress increases with the crack size. PEEQ exhibits the opposite trend. When the initial crack size $a = 5$ mm, the stress at the crack tip front does not reach the yield value, and the equivalent plastic strain is 0. A typical example is that when the crack growth is dominated by stress at $a = 10$ mm, where the stress values are 458.862 MPa and 511.73 MPa, and when the angles between the taking point and the crack are −68° and 65°, respectively. If initial crack growth occurs at the 52 Mb/52 Mw interface, the crack is likely to grow in direction −68° or 65° from the initial crack angle, and the crack is more likely to propagate to the 52 Mw side, as shown in Figure 17(a). Conversely, when crack growth is dominated by PEEQ, the crack tends to propagate towards the 52 Mb side, as shown in Figure 17(b).

Figure 18 shows the magnitude of the crack tip front stress and PEEQ at the 52 Mw/316L interface. The local region of the crack tip is less affected by mechanical heterogeneity because of the small difference in the yield strength distribution near this interface. Taking the maximum crack size ($a = 10$ mm) as an example, when crack growth is dominated by stress, the stress values are 509.291 and 510.21 MPa when the angles between the taking point and the crack are 67° and −67°, respectively. Since the stress
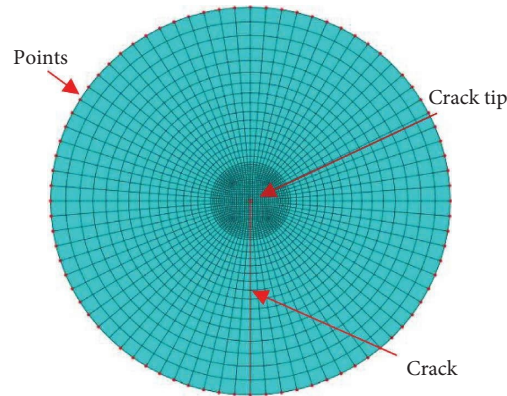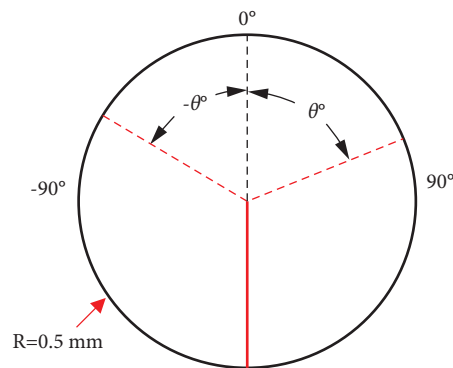
FIGURE 14: Selection of data points.

FIGURE 15: Definition of the crack angle.

magnitude is almost the same on both sides, if the initial crack growth occurs at this interface, the crack is likely to spread in direction ±67°, as shown in Figure 18(a). Due to the near symmetrical stress and strain on both sides of the crack, their effects are identical. This leads to equal constraint effects on both sides, which cancel each other out; thus, the crack is likely to propagate along a straight line (0°).

In summary, the mechanical heterogeneity of DMWJs and the initial crack depth affect the local mechanical field in front of the crack tip, which may further affect the crack propagation direction. Specifically, the larger the initial crack, the greater the possibility of crack initiation and growth.

3.4. Local Mechanical Behavior of SA508/52 Mb and 52 Mw/ 316L Interface Regions. To investigate the mechanical behavior of the interface areas on a local scale, the cracks were positioned at various distances from the interface. In the SA508/52 Mb local region, the cracks were placed in the SA508 region ($y = -6, -5, -4, -3, -2, -1$, and -0.5 mm), on the SA508/52 Mb interface ($y = 0$ mm), and in the 52 Mb region ($y = 0.5, 1, 2, 3, 4$, and 5 mm). For comparison with the continuous transition model, four single homogeneous material (SA508, 52 Mb, 52 Mw, and 316L) specimens with the same geometry, mesh, load, and boundary conditions as the

dissimilar welded joint were used for the analysis, respectively, as shown in Figures 19 and 20 (indicated by arrows).

Figure 19 shows the stresses and PEEQ of the crack tips at different crack initial locations in the SA508/52 Mb interface area. The stress and PEEQ vary with the initial locations of the crack and are most significant in HAZ. The higher stress and PEEQ are situated roughly at the SA508/ 52 Mb near-interface region ($y = -0.5$ mm); therefore, this should be the weakest point of the near-interface region. When the initial location of the crack is within the SA508 region of BM, the stress and PEEQ of the crack tip gradually stabilize with increasing distance from the interface ($y = 0$ mm). When the crack is $y = -4$ mm from the interface, the stress and PEEQ of the crack tip are essentially the same as those of the crack tip in the homogeneous material (the arrows in Figure 19 identify the stress and PEEQ of the crack tip in the homogeneous materials). When the initial position of the crack is located in Alloy52 Mb ([0, 2]), the stress at the crack tip gradually decreases and stabilizes and PEEQ at the crack tip first decreases and then increases and stabilizes. Within 52 Mb at $y = 2$ mm from the interface, the stresses and plastic strains at the crack tip are essentially the same as those in the homogeneous material. Therefore, the stress and strain
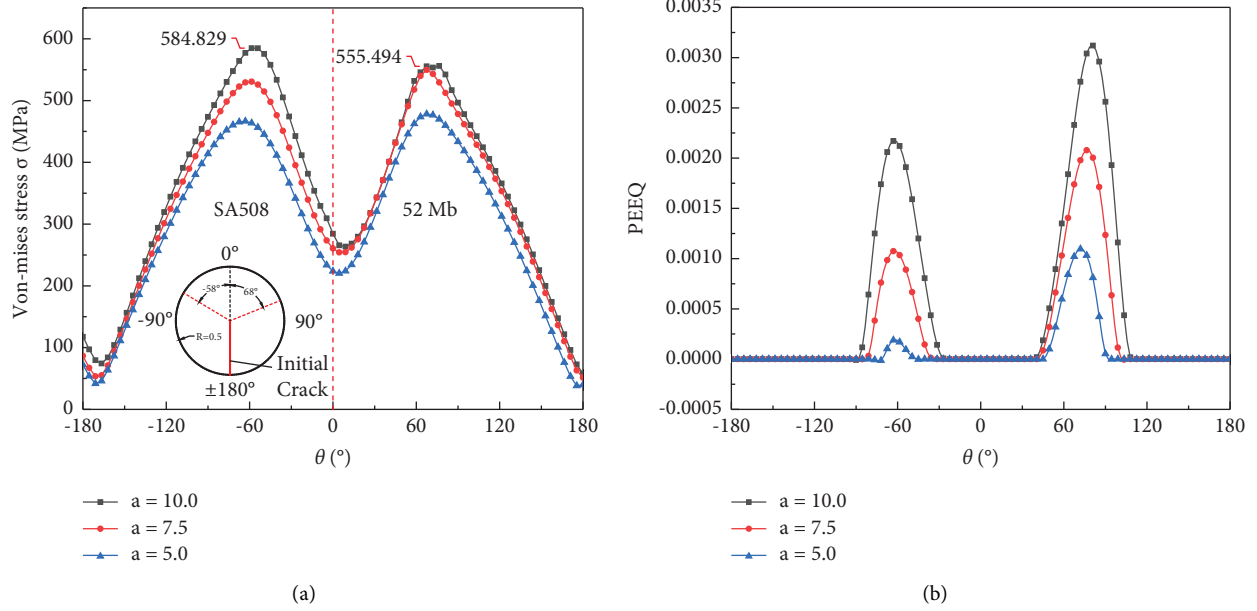
Figure 16: The crack tip at the SA508/52Mb interface: (a) von Mises stress; (b) PEEQ.
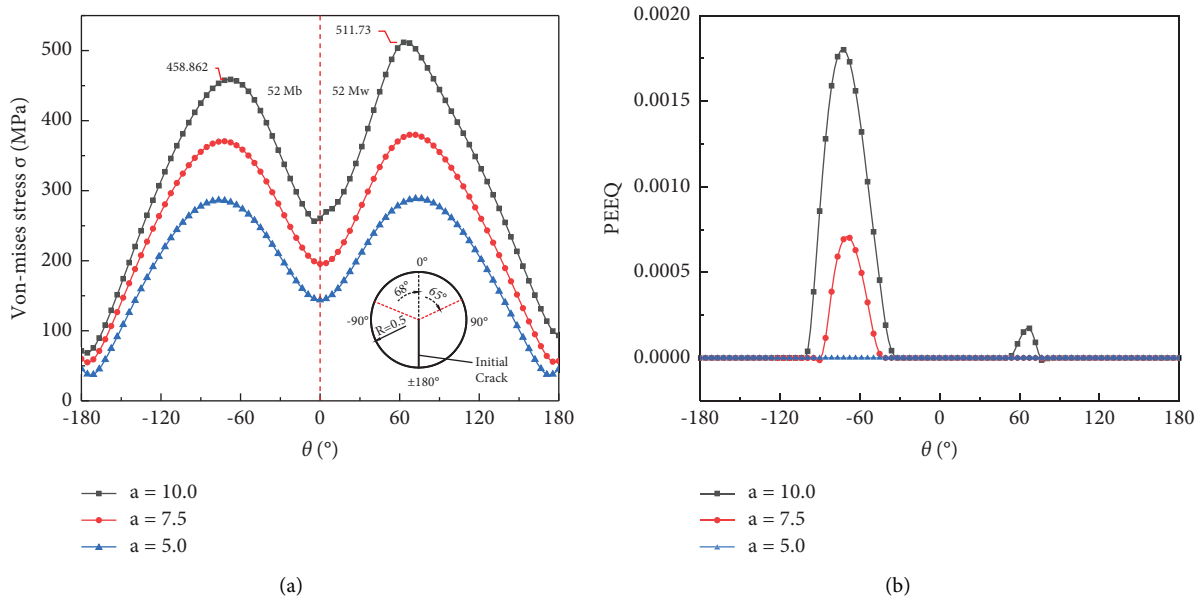

Figure 17: The crack tip at the 52Mb/52Mw interface: (a) von Mises stress; (b) PEEQ.

at the crack tip in the interval from $y = -4$ mm to $y = 2$ mm in the SA508/52 Mb interface region vary significantly. This variation may be caused by the mechanical heterogeneity at different locations.

The abovementioned results show that the material constraint effect caused by heterogeneous mechanical properties causes the stress and PEEQ at the crack tip to vary based on the initial locations of the cracks. Stresses in the SA508/52 Mb interface region are lower than those in homogeneous SA508, specifically from $y = -0.5$ mm to $y = -4$ mm. This material constraint effect can restrain crack initiation and propagation and contribute to the reliability of the welded

structure, and this positive effect reaches its maximum when $y = -3$ mm. Meanwhile, when $y < -4$ mm, the material constraint effect vanishes, and the stress and plastic strain are identical to those in the homogeneous material.

Figure 20 shows the stresses and PEEQ of the crack tips at different initial crack locations in the 52 Mw/316L interface region. In the local area, the crack tip exhibits a relatively higher stress and plastic strain in the vicinity of the 52 Mb/316L interface ($y = 0$ mm). When the crack is in Alloy52 Mw, the stress and PEEQ at the crack tip gradually decrease ($y = 0$ mm to $y = -3$ mm) and stabilize as the crack moves away from the interface ($y = 0$ mm). Meanwhile, when
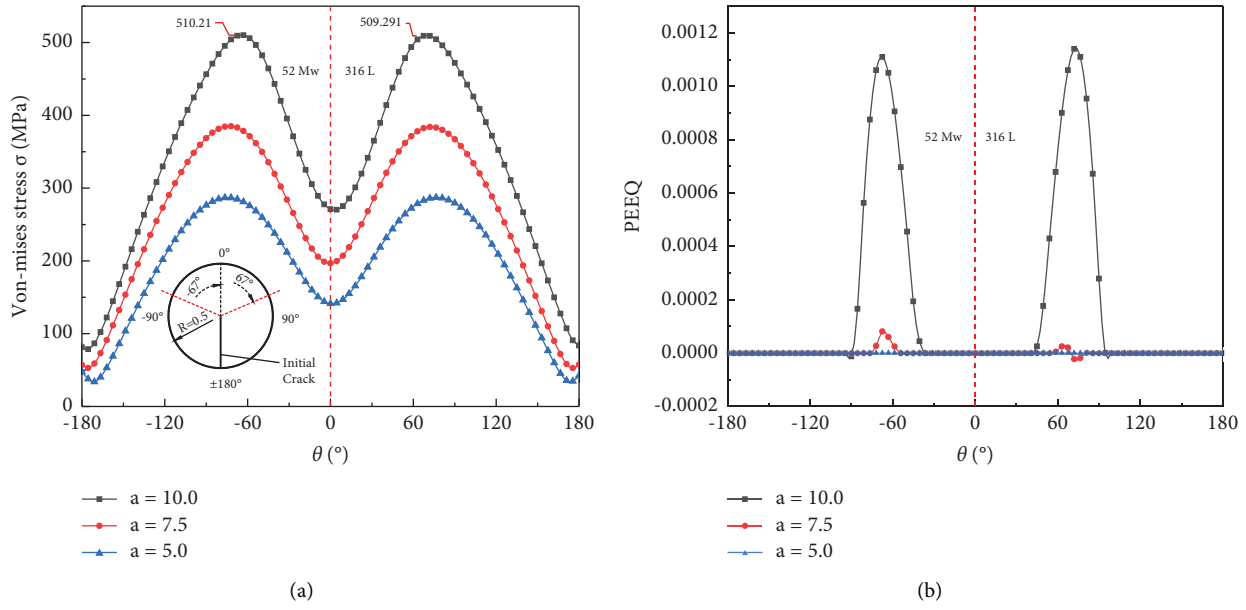
FIGURE 18: The crack tip at the 52Mw/316L interface: (a) von Mises stress; (b) PEEQ.
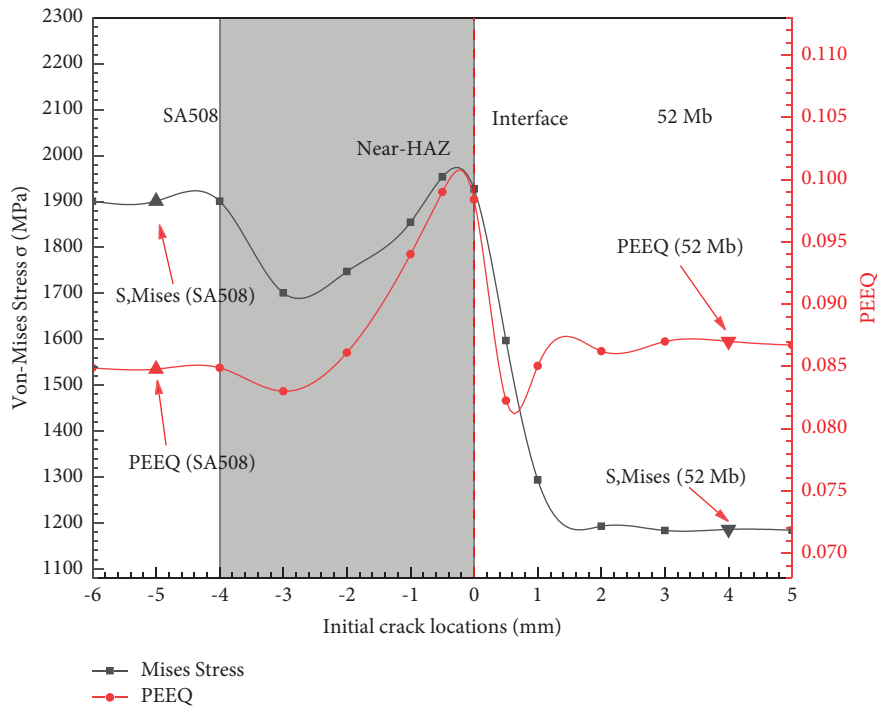

FIGURE 19: Stress and strain at different initial locations of cracks in the SA508/52Mb interface region.

the crack is at $y = -4$ mm, the stress and PEEQ at the crack tip are essentially the same as those in the homogeneous material (the arrows in Figure 20 identify the stress and plastic strain at the crack tip in the homogeneous materials). When the crack is in 316L, the changes in the stress and PEEQ in the crack tip are more significant from $y = 0$ mm to $y = 8$ mm. At distance $y > 8$ mm, the stresses and plastic strains at the crack tip are essentially the same as those in the

homogeneous materials. Therefore, the stress and strain at the crack tip in the interval from $y = -3$ mm to $y = 8$ mm in the 52 Mw/316L interface region vary significantly. This variation may be caused by the mechanical heterogeneity at different locations.

The abovementioned results show that when $y = 0$ mm to $y = 8$ mm, the stress in the 52 Mw/316L interface region is higher than that in the homogeneous material. This material
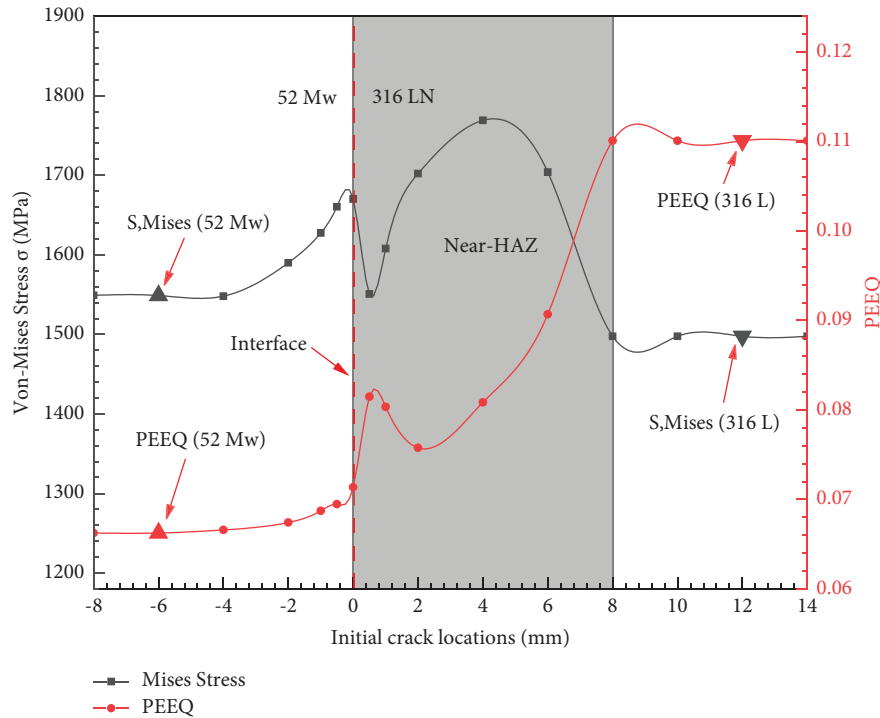
FIGURE 20: Stress and strain at different initial locations of cracks in the 52Mw/316L interface region.

constraint effect can promote crack initiation and growth, which will have a negative impact on the reliability of the welded structure, and this negative effect reaches its maximum when $y = 4$ mm. When $y > 8$ mm, the material constraint effect vanishes and the stress and plastic strain behave almost identically to those in a homogeneous material.

4. Conclusion

The stress and plastic strain conditions at the crack tip in mechanically heterogeneous DMWJs and the mechanical behavior of the interface regions were investigated via FEM numerical analysis based on a UMAT model. The main conclusions are as follows:

(1) The inhomogeneous distribution of mechanical properties (strength and work-hardening properties) around the crack determines the stress and plastic strain in front of the crack tip, which may further influence the direction of interfacial crack growth. The mechanical condition of the crack tip can be affected by the crack size; the larger the crack, the more likely it is that crack initiation and growth will occur.

(2) Both the SA508/52 Mb and 52 Mw/316L interface cracks have high stress and plastic strain. The higher stress and plastic strain promote crack initiation and growth, and hence, the near-interface region is often the weak point where damage occurs.

(3) In the BM near the SA508/52 Mb interface, the material constraint effect induced from mechanical heterogeneity inhibits crack initiation and growth,

thereby enhancing the reliability of the welded structure. Meanwhile, in the BM near the 52 Mw/316L interface, the constraint effect induced from mechanical heterogeneity promotes crack initiation and growth, which reduces the reliability of the welded structure.

(4) The mechanical heterogeneity between 52 Mw and 316L resulted in a larger HAZ width. Therefore, the range of mechanical behavior changes in the 52 Mw/316L interface region is larger than those of the SA508/52 Mb interface region. For safety assessment, it is recommended to determine and utilize mechanical properties associated with the crack sites.

Future research in this field should include the prediction of the crack propagation rate in the interface region and the fracture resistance behavior in DMWJs.

Data Availability

The mechanical field data used to support the findings of this study are included within the article.

Conflicts of Interest

The authors declare that there are no conflicts of interest.

Acknowledgments

References

[1] H. Xue, K. Ogawa, and T. Shoji, "Effect of welded mechanical heterogeneity on local stress and strain ahead of stationary and growing crack tips," *Nuclear Engineering and Design*, vol. 239, no. 4, pp. 628–640, 2009.

[2] H. T. Wang, G. Z. Wang, F. Z. Xuan, and S. T. Tu, "Numerical investigation of ductile crack growth behavior in a dissimilar metal welded joint," *Nuclear Engineering and Design*, vol. 241, no. 8, pp. 3234–3243, 2011.

[3] H. T. Wang, G. Z. Wang, F. Z. Xuan, and S. T. Tu, "Fracture mechanism of a dissimilar metal welded joint in nuclear power plant," *Engineering Failure Analysis*, vol. 28, pp. 134–148, 2013.

[4] P. L. Andresen, "A brief history of environmental cracking in hot water," *Corrosion*, vol. 75, no. 3, pp. 240–253, 2019.

[5] O. K. Chopra, H. M. Chung, T. F. Kassner et al., "Current research on environmentally assisted cracking in light water reactor environments," *Nuclear Engineering and Design*, vol. 194, no. 2-3, pp. 205–223, 1999.

[6] L. J. Dong, C. Ma, Q. J. Peng, E. H. Han, and W. Ke, "Microstructure and stress corrosion cracking of a SA508-309L/308L-316L dissimilar metal weld joint in primary pressurized water reactor environment," *Journal of Materials Science and Technology*, vol. 40, pp. 1–14, 2020.

[7] H. T. Wang, G. Z. Wang, F. Z. Xuan, C. J. Liu, and S. T. Tu, "Local mechanical properties of a dissimilar metal welded joint in nuclear power systems," *Materials Science and Engineering A*, vol. 568, pp. 108–117, 2013.

[8] P. Štefane, S. Naib, S. Hertelé, W. De Waele, and N. Gubeljak, "Crack tip constraint analysis in welded joints with pronounced strength and toughness heterogeneity," *Theoretical and Applied Fracture Mechanics*, vol. 103, Article ID 102293, 2019.

[9] H. Xue, Y. Q. Bi, S. Wang, J. Zhang, and S. Gou, "Compilation and application of UMAT for mechanical properties of heterogeneous metal welded joints in nuclear power materials," *Advances in Materials Science and Engineering*, vol. 2019, Article ID 3151823, 12 pages, 2019.

[10] K. Fan, G. Z. Wang, J. Yang, F. Z. Xuan, and S. T. Tu, "Numerical analysis of constraint and strength mismatch effects on local fracture resistance of bimetallic joints," *Applied Mechanics and Materials*, vol. 750, pp. 24–31, 2015.

[11] L. Dong, Q. Peng, E. H. Han, W. Ke, and L. Wang, "Microstructure and intergranular stress corrosion cracking susceptibility of a SA508-52 M-316L dissimilar metal weld joint in primary water," *Journal of Materials Science and Technology*, vol. 34, no. 8, pp. 1281–1292, 2018.

[12] J. L. Gan, Y. Peng, and J. Dong, "The effect of the heterogeneous pattern of material mechanical properties on the structural performance analysis of butt joints," *Progress in Steel Building Structures*, vol. 19, pp. 41–46, 2017.

[13] H. Altenbach, J. Altenbach, and W. Kissing, *Mechanics of Composite Structural Elements*, Springer Nature Singapore Pte Ltd, Singapore, 2nd edition, 2018.

[14] T. Sarikka, M. Ahonen, R. Mouginot et al., "Microstructural, mechanical, and fracture mechanical characterization of SA 508-Alloy 182 dissimilar metal weld in view of mismatch state," *International Journal of Pressure Vessels and Piping*, vol. 145, pp. 13–22, 2016.

[15] C. Lu, M. Zhao, L. Jie et al., "Stress distribution on composite honeycomb sandwich structure suffered from bending load," *Procedia Engineering*, vol. 99, pp. 405–412, 2015.

[16] A. Szekrényes, "Analytical solution of some delamination scenarios in thick structural sandwich plates," *Journal of Sandwich Structures and Materials*, vol. 21, no. 4, pp. 1271–1315, 2019.

[17] J. Yang and L. Wang, "Fracture mechanism of cracks in the weakest location of dissimilar metal welded joint under the interaction effect of in-plane and out-of-plane constraints," *Engineering Fracture Mechanics*, vol. 192, pp. 12–23, 2018.

[18] K. Fan, G. Z. Wang, F. Z. Xuan, and S. T. Tu, "Local failure behavior of a dissimilar metal interface region with mechanical heterogeneity," *Engineering Failure Analysis*, vol. 59, pp. 419–433, 2016.

[19] R. Guo, H. Xue, and X. Y. Gong, "Influence of residual stress and heterogeneity on mechanical field at crack tips in safety end of nuclear power plant," *Procedia Structural Integrity*, vol. 13, pp. 2202–2209, 2018.

[20] H. T. Wang, G. Z. Wang, F. Z. Xuan, and S. T. Tu, "An experimental investigation of local fracture resistance and crack growth paths in a dissimilar metal welded joint," *Materials and Design*, vol. 44, pp. 179–189, 2013.

[21] K. Fan, G. Z. Wang, F. Z. Xuan, and S. T. Tu, "Local fracture resistance behavior of interface regions in a dissimilar metal welded joint," *Engineering Fracture Mechanics*, vol. 136, pp. 279–291, 2015.

[22] U. Zerbst, R. A. Ainsworth, H. T. Beier et al., "Review on fracture and crack propagation in weldments–A fracture mechanics perspective," *Engineering Fracture Mechanics*, vol. 132, pp. 200–276, 2014.

[23] L. Y. Zhao, Y. H. Cui, and H. Xue, "Effect of mechanical heterogeneity on the crack driving force of a reactor pressure vessel outlet nozzle DMW joint," *IOP Conference Series: Materials Science and Engineering*, vol. 280, pp. 012–031, 2017.

[24] S. Y. Yang, "Conversion of ABAQUS user material subroutines," *Journal of the Computational Structural Engineering Institute of Korea*, vol. 23, pp. 635–640, 2010.

[25] D. C. Lu, X. L. Du, G. Wang, A. N. Zhou, and A. K. Li, "A three-dimensional elastoplastic constitutive model for concrete," *Computers and Structures*, vol. 163, pp. 41–55, 2016.

[26] J. Kim and D. N. Kim, "Robust stress integration algorithms for implicit elastoviscoplastic finite element analysis of materials with yield-point phenomenon," *International Journal of Mechanical Sciences*, vol. 150, pp. 277–289, 2019.

[27] D. Liao, Z. X. Yang, and T. T. Xu, "J2-deformation-type soil model coupled with state-dependent dilatancy and fabric evolution: multiaxial formulation and FEM implementation," *Computers and Geotechnics*, vol. 129, Article ID 103674, 2021.

[28] W. K. Wang, Y. Liu, Q. B. Zhang, L. J. Zhang, and J. X. Zhang, "Microstructure and local mechanical properties of a dissimilar metal welded joint with buttering layer in steam turbine rotor," *Materials Science and Engineering: A*, vol. 747, pp. 244–254, 2019.

[29] Y. Peng, C. Wu, J. Gan, and J. Dong, "Characterization of heterogeneous constitutive relationship of the welded joint based on the stress-hardness relationship using microhardness tests," *Construction and Building Materials*, vol. 202, pp. 37–45, 2019.

[30] H. Ming, R. Zhu, Z. Zhang et al., "Microstructure, local mechanical properties and stress corrosion cracking susceptibility of an SA508-52 M-316LNsafe-end dissimilar metal weld joint by GTAW," *Materials Science and Engineering A*, vol. 669, pp. 279–290, 2016.

[31] R. F. Liu and J. C. Wang, "Finite element analyses of the effect of weld overlay sizing on residual stresses of the dissimilar metal weld in PWRs," *Nuclear Engineering and Design*, vol. 372, Article ID 110959, 2021.

[32] H. Xue, Z. Wang, S. Wang, J. X. He, and H. L. Yang, "Characterization of mechanical heterogeneity in dissimilar metal welded joints," *Materials*, vol. 14, no. 15, p. 4145, 2021.